



Photoactivity of TiO₂ nanoparticles covered with nitro group in Fluoxetine and Rhodamine-B degradation

Ailton J. Moreira^a, Shena R.R. Padilha^a, Vagner R. de Mendonça^b, Elaine C. Paris^c,
Caue Ribeiro^c, Gian P.G. Freschi^a, Tania R. Giraldi^{a,*}

^aFederal University of Alfenas, Poços de Caldas Campus, Rod. José Aurélio Vilela, BR 267, Km 533, 11999 – University City, Poços de Caldas – MG, Zip Code: 37715-40, Brazil, Tel. +55 35 3697-4600; emails: tania.giraldi@unifal-mg.edu.br (T.R. Giraldi), aijomoquim@gmail.com (A.J. Moreira), shena_rrp@hotmail.com (S.R.R. Padilha), gianpgfreschi@gmail.com (G.P.G. Freschi)

^bFederal Institute of Education, Science and Technology of São Paulo – Itapetininga Campus João Olímpio de Oliveira Avenue, 1561, Vila Asem – Itapetininga-SP, Zip Code: 18208-000, Brazil, email: vagneromito@yahoo.com.br (V.R. de Mendonça)

^cEmbrapa Instrumentação Agropecuária, Rua XV de Novembro, 1452, São Carlos-SP, Zip Code: 13560-970, Brazil, emails: elaine.paris@embrapa.br (E.C. Paris), caue.ribeiro@embrapa.br (C. Ribeiro)

Received 10 February 2020; Accepted 22 July 2020

ABSTRACT

TiO₂ nanoparticles and TiO₂ covered with nitro groups were prepared. Nanoparticles with diameters of 15–25 nm were obtained, consisting 100% of the anatase phase (for heat treatment of 450°C) and some peaks referring to the rutile phase (for heat treatment of 500°C). The X-ray diffraction and Raman spectroscopy analysis showed crystalline structure without deformations, indicating that the nitro groups present on the surface did not influence these properties. Infrared spectra showed the presence of nitro groups on the surface of the semiconductor (450TiN12), which resulted in degradation of 70% compared to photolysis when applied in the Rhodamine B photodegradation. The semiconductors were then applied in the fluoxetine (FLX) degradation. The pH monitoring showed that TiO₂ covered with nitro groups, and treated at 450°C for 12 h, resulted in increased deprotonation (above 100%) when compared to the process using pure TiO₂. The studies permitted defining the behavior of the FLX degradation and the understanding of the mechanism resulting from the insertion of TiO₂ covered with nitro groups (electrophiles), which interact with the FLX (nucleophile) amino group promoting its deprotonation. These results can be used in the design of new materials to be applied in pharmaceutical photodegradation.

Keywords: TiO₂; Fluoxetine; Surface modification; Nanomaterials; Photocatalysis

1. Introduction

Titanium oxide, one important functional compound, has attracted considerable interest owing to their applications in catalysis, photochemical solar cells, controlled release, chemical sensors, biodiesel production, and so on [1–8]. In catalysis, a particular case is the photochemical oxidative process, in which a semiconductor surface is activated by UV-light to generate free radicals from

OH[•] adsorbed species. These radicals are responsible for the degradation of contaminants such as organic molecules [9], pesticides [10,11], and pharmaceuticals [12,13]. Several factors can interfere in the catalytic activity of this material, for example, the method of synthesis [14], the presence of surface contaminants [15–17], particle shapes [18], counter ions from precursors used in synthesis [17], among others.

Research has been reported on the preparation and characterization of TiO₂ materials doped with impurities such as transition metals [18,19] or main elements like

* Corresponding author.

carbon [20,21], nitrogen [22,23], and sulfur [24,25]. The goal is to enable more efficient use of such catalysts. However, a dopant promotes not only improvement in photocatalytic activity but also modification in the crystalline structure, shape and particle sizes. Weber et al. [26] propose that the presence of the additional element alters the particle growth behavior. Considering that particle growth is controlled simultaneously by a thermodynamic and a kinetic factor, the introduction of dopant into the systems changes either the surface energy or the boundary mobility of the particles. Duarte et al. [27] developed N-TiO₂ thin films and verified smaller particle sizes in thicker films. Authors attribute this surface modification to the fact of nitrogen decreasing the mobility of Ti and O. Then the diffusion process decreased, and deep valleys between grain boundaries were generated, and, as consequence, increased the effective surface area.

The efficiency of photocatalytic reactions is related with the TiO₂ band-gap and the degree of electron-hole recombination in the process, as well as by the limited adsorption capability of photocatalysts. It is generally expected that the photocatalyst has a high surface area and a contaminant-free surface to promote a greater number of active sites to start the photocatalytic process [28,29]. However, studies are focused on TiO₂ surface modification, including surface derivation with ascorbic acid, polymer [30], urea/rhodamine B (RhB)-capped TiO₂ nanoparticles [31], complex (Tiron-TiO₂) [32], or even activated carbon coating [33].

Xing et al. [34] modified the surface of TiO₂ particles by chemical adsorption in saturated solution of salicylic acid. After the surface modification, the wavelength response range of TiO₂ was expanded. The efficiency of 4-nitrophenol degradation increased from 39.5% to 79.3% after surface modification. Compared with the pure TiO₂, surface modification led not only to improving the surface coverage of 4-nitrophenol, but also to increasing the light utilization. Both of these factors were important for the photocatalytic activity in photocatalysis process. Bossmann et al. [30] compared the photocatalytic activity of TiO₂ conventional and modified with a 4,4'-bipyridinium monolayer in this surface (V²⁺-TiO₂). Authors investigated the efficiency of degradation of a series of organic compounds, among them, 2,4-xylidine. The formation of intermediate 2,4-dimethylphenol was evidenced, indicating that the major pathway of substrate oxidation proceeds is via electron transfer from the adsorbed aromatic compounds to the "holes" within the valence band of the semiconductor. The efficiencies of photocatalytic degradation by both V²⁺-TiO₂ and TiO₂ were limited by the trapping efficiency of the conduction band electrons by molecular oxygen.

Hadjiivanov et al. [35] verified the presence of nitro groups on the surface of the anatase TiO₂, that was confirmed by the appearance of absorption bands in the region of 1,630 cm⁻¹ of the Fourier transform infrared (FTIR) spectrum. Also, according to Zhang and Cole [36], the anchoring of nitro groups in nanomaterials is not simple, but these can promote influences in reactional processes, since they are very electrophilic groups. Pap et al. [37] obtained TiO₂ covered with nitro groups with different times of thermal treatments, promoting the surface of the catalyst-free, allowing new interactions in photocatalytic processes. Although the

literature reports some studies with TiO₂ covered with nitro groups, these are not applied in photocatalytic processes.

Importantly, the processes of emergent contaminants degradation has been evaluated as a function of the products resulting from the degradation of the original compound, as these by-products may increase [38,39] or decrease [40] the toxicity of the treated effluent. According to Pinto et al. [41], fluoxetine (FLX) exhibits high thermal stability below 170°C, besides persistence in the environment. In their studies, Yin et al. [42] found a half-life of 70–145 d for FLX under different experimental conditions, determining that photolytic and hydrolytic processes contribute to the degradation of the compound.

Due to the stability of the compound, new processes have been investigated, where a 15% increase of degradation was verified with the insertion of semiconductor Degussa P25 and TiO₂ZnSiO₂ obtained from petrochemical residue [43]. In solar photocatalytic degradation (TiO₂), 22 drugs were evaluated, 19 of which (FLX and others) were completely degraded [44]. Applying TiO₂ to drug degradation, achieved degradation above 60% of FLX by applying LED lamp as a photon emitter (365 nm) [45] and achieved values of 90% FLX degradation using TiO₂ and UV radiation [46].

For the different processes of FLX degradation (photocatalysis, ozonolysis, and electrochemical processes) [47–49], different by-products can be formed, and the monitoring of these is necessary, since it allows to unravel the degradation mechanisms, and to understand more concretely the kinetic processes. In general, the literature has shown that the mechanisms of FLX degradation can occur via hydroxylation [50], dealkylation [48] and dehalogenation [40], and evaluating the influence of different semiconductors on the FLX degradation processes is important for understanding their pathways of degradation and selectivity in the by-products formation.

The central idea of the present paper was to investigate the influence of nitro groups on the surface of the TiO₂ photocatalyst. To the best of our knowledge, there aren't data in literature reporting the influence of nitro groups on the semiconductor surface in photocatalytic activities. The generation of these groups on the surface was promoted by means of chemical reactions, from urea added in the reaction medium, since that urea is an innocuous raw material, which may be hydrolyzed to form ammonia and carbon dioxide gases [51]. Ammonia could be oxidized to NO_x [52], and with high temperatures facilitating this conversion. This fact motivated the present study, since the ammonia produced from the decomposition of the urea can be converted to NO_x by the heat treatment. Therefore, in order to investigate different processes of semiconductor synthesis and their application in photocatalytic processes, TiO₂ nanoparticles were synthesized by polymeric precursor method [53] with and without urea in reactive means, and tested as catalysts in the Rhodamine-B photodegradation. The samples were submitted to different heat treatments in order to observe the annealing effects on the photocatalytic properties, surface decontamination, and the consequent structural and morphological changes. Finally, the best sample was utilized to investigate the FLX photodegradation.

2. Experimental

2.1. Synthesis of nanoparticles

Ti⁴⁺ solutions were prepared by the polymeric precursor method. This method consists in dissolving titanium tetraisopropoxide (Sigma-Aldrich, St. Louis, MO, EUA) in an aqueous solution of citric acid (Merck, Darmstadt, Germany) at 75°C in a molar ratio of 1:3. Here, 7.2 g of citric acid (Alfa Aesar, Tewksbury, MA, USA) was added in distilled water until complete dissolution. Then titanium isopropoxide was added to this solution and kept under stirring for 24 h, whereby the titanium citrate was formed. Titanium citrate obtained was polymerized by the addition of 4.2 mL of ethylene glycol (Merck, Darmstadt, Germany). The mixture was kept under stirring and heating at 70°C for 1 h to ensure formation of the polymer. Samples with nitrogen was obtained in the same way by adding to 9 g of urea (synth) in the citric acid solution. The solutions were firstly annealed at 300°C in a conventional electric oven for 2 h in order to promote pyrolysis. The remaining material was divided in six equal portions and each of them was submitted to different calcination temperatures (450°C and 500°C) and times (2, 12, and 24 h) at 1 C min⁻¹ heating rate, to produce the N-TiO₂ nanoparticles. The samples received the abbreviations XTiNY, where X is the heat treatment temperature, TiN is relative to Ti:N ratio, and Y is the heat treatment time.

2.2. Characterization

The structural characterization was assessed by X-ray diffraction (XRD). The analyses were performed on a Shimadzu XRD-6000 (Tokyo, Japan) with operating voltage of 40 kV, current of 30 mA, scan angular range of 20°–60° (2θ interval) and a 1° min⁻¹ displacement. The Raman spectra were collected (FT Raman Bruker RFS100/S, Tokyo, Japan) using the 1,064 nm line of a 450 W YAG laser; 200 scans were used for each measurement at room temperature. KBr-pellets were examined by infrared spectroscopy technique in a Bruker Vertex 70 spectrophotometer. The FTIR spectra were obtained with 32 scans and 4 cm⁻¹ resolution in the 4,000 at 450 cm⁻¹ range. Elemental CHNS analysis of the samples was performed using 2400 series II CHNS/O elemental analyzer, Perkin Elmer, (Waltham, MA, EUA). The determination error of N is <0.1%. The morphology and the particle size were investigated by field emission gun scanning electron microscopy (FEG-SEM) using the JEOL JSM6701F equipment (Peabody, MA, EUA). Since the silicon plate disposed over silver was not suitable for visualizing the particles distinctly, the sample ports were coated with carbon paint. The powders were dispersed in acetone, deposited in the sample ports and later dried at 100°C. The zeta potential was measured in the materials suspension at pH 6.0 (natural) by electrophoretic light scattering, using a Malvern Zetasizer NanoZS potential and particle size analyzer (Worcestershire, United Kingdom). Finally, the samples were subjected to diffuse reflectance analysis, and the band gap was calculated by the Kubelka–Munk model.

2.3. RhB photocatalytic essays

RhB (synth) was used as a probe dye for the photocatalytic essays. Suspensions containing 5 mg of particles

in 50 mL of RhB solution (5.0 mg L⁻¹) were prepared and irradiated during 180 min. Photocatalytic experiments in the UV region were performed in a glass beaker, placed in a wooden reactor. Its internal dimensions were 45 cm (length) × 20 cm (width) × 28 cm (height) and 23 cm height between the lamp and the solution to be irradiated. In addition, it also consisted of four low-pressure mercury Philips lamps (Amsterdam, Netherlands) TUV 15W/G15T8 – Long Life – UV – C (λ_{max} = 254 nm), 1 cooler axial AC FAN model FZY8038 MBL and copper serpentine coupled coil to ultratermostatic bath SL 152/18 – SOLAB 2000W/220V with water pump and with temperature control in 20°C.

The reduction in dye concentration was estimated based on color removal, which was determined by spectrophotometry (Cary 60 UV-vis, da Agilent spectrophotometer, Santa Clara, CA, EUA) at various light exposure times. Blank experiments were carried out in RhB solution without particles (direct photolysis).

2.4. FLX photolytic and photocatalytic essays

Standard solution (stock) of FLX 98,49% (Santa Cecilia Pharmacy, Poços de Caldas, MG, Brazil) and 4-(trifluoromethyl)phenol (TFMP) 97% (Sigma-Aldrich, St. Louis, MO, EUA) 1,000 mg L⁻¹ were prepared by dissolving the respective reagents in methanol high performance liquid chromatography (HPLC) grade (Jt Backer, Center Valley, PA, EUA). A phosphate buffer solution pH = 3.0 (10.0 mmol L⁻¹ KH₂PO₄) was prepared by dissolving the respective salts (Sigma-Aldrich, St. Louis, MO, EUA), adjusting the pH with phosphoric acid 85% (Neon).

Acetonitrile and methanol, HPLC grade (JT Backer) were used in the preparation of solutions and processes linked to chromatographic analysis. Standard solutions of FLX were prepared in ultrapure water and not in environmental matrices. All solutions were prepared from analytical grade chemicals and ultra-pure water with a minimum of 18.0 M⁻¹ Ω cm resistivity obtained in a Milli-Q Plus system (Millipore, Bedford, MA, USA). The samples/standards were stored in high density polypropylene bottles (Nalgene®) and were kept refrigerated.

Photolytic experiments in the UV region were performed in reactor describe in item (2.3). For the photocatalytic study, 5 mg of the TiO₂ and 450TiN12 samples and 10 mL of the FLX sample 10.0 mg L⁻¹ (pH = 5.95) are added in 50 mL glass beaker and taken to UV reactor for irradiation (constant stirring). Samples were irradiated in the time interval of 5–120 min. After irradiation, samples were filtered in 0.45 μm filters for removal of the catalysts and subjected to chemical analysis by high performance liquid chromatography with UV detection, potentiometry with a selective ion electrode for determination of fluoride, and pH analysis through electrode of glass membrane.

The chromatographic analyses were performed on a HPLC Agilent 1220 infinity LC (Santa Clara, CA, EUA) equipped with an automatic injector, an oven temperature control column, a UV/vis detector system (225 nm) and a chromatographic column Zorbax Eclipse plus C18, 4.6 mm × 250 mm, 5 μm. The chromatographic conditions were: elution gradient (v/v): 0 min, 50% (ACN)/50% PO₄³⁻ buffer (pH = 3); 0–1 min, 45% (ACN)/55% PO₄³⁻ buffer (pH = 3); 1–4 min, 75% (ACN)/25% PO₄³⁻ buffer (pH = 3); 4–5 min, 90%

(ACN)/10% PO_4^{3-} buffer (pH = 3); 5–7 min, 100% (ACN)/00% PO_4^{3-} buffer (pH = 3), detecting 225 nm, a mobile phase flow rate of 1 mL min^{-1} , and a temperature control of 35°C.

The processing of chromatographic data was administered by the Agilent OpenLAB (Santa Clara, CA, EUA) chromatography data system software (CDS) EZChrom. Also in this step, another aliquot of the sample was sent for quantification of fluoride through the potentiometry with fluoride selective ion electrode (Agilent, Santa Clara, CA, EUA), and for this analysis, the ionic strength of the solution was adjusted with acetate buffer.

3. Results

3.1. Characterization of nanomaterials

Fig. 1a shows the XRD patterns of the particles annealed at different heat treatment conditions. The diffraction peaks of the TiO_2 polymorphs anatase (JCPDS n°. 21-1272) and rutile (JCPDS n°. 21-1276), were indexed to their respective crystallographic planes. The peaks for rutile were verified in the samples heated to 500°C. It was also verified that pure

TiO_2 presented higher crystallinity than N- TiO_2 heated at 450°C. It is believed that the reducing atmosphere created by the decomposition of urea delayed crystallization. However, with the increase of the treatment temperature to 500°C, the samples showed higher crystallinity, which can be evidenced by the narrowing and increase of peak intensity. Since there aren't dislocations in the XRD peaks, the doping process can be disregarded.

Fig. 1b shows Raman shifts of the as prepared samples. Raman spectra are in good agreement with those spectra reported earlier for titanium oxide in the anatase phase. The anatase phase shows major Raman bands at 143, 197, 396, 516, and 639 cm^{-1} . These bands can be attributed to the Raman-active modes of the anatase phase with the symmetries of Eg, B1g, A1g/B1g, and Eg, respectively [54].

In order to check the nanoparticles morphology, we performed FEG-SEM analysis and the results were shown in Fig. 2. Accordingly, the particles presented nanometric shapes, a remarkable feature of the synthesis methodology applied in this study. The presence of agglomerates/aggregates in particles submitted to higher heat treatment temperatures was identified (500TiN12 and 500TiN24). These samples presented irregular morphology and higher particle size (20 and 25 nm, respectively). It was also observed that N- TiO_2 samples presented smaller particle size in the same conditions of thermal treatment (450TiN12) compared to TiO_2 . Therefore, we can state that covering the particles avoids their growth.

As a matter of fact, Table 1 shows the crystallite size of the samples, calculated by the Scherrer's equation, and average particle size obtained by FEG-SEM analysis. By comparing the samples treated at the same temperature, but in different times, it can be seen that a sintering process took place, yielding in larger particles when longer times (24 h) were applied. It is interesting that crystallite size barely changed with the treatment time, that is, probably occur an increasing the number of crystallites per particle. Analysing the effect of temperature, it can be noted that the increase in crystallite size is less pronounced than the increase in particle size, corroborating the analysis previously done.

Since the aim of the synthesis method was to modify the surface of the as-synthesized materials with nitro groups, we performed FTIR analysis and the results are presented in Fig. 3a. In order to have an unambiguous conclusion, we also performed CHNS analysis trying to estimate the amount of nitrogen in the samples.

It is observed that TiO_2 does not present bands referring organic compounds. Besides, the samples show bands at 1,633 cm^{-1} , which are related to asymmetrical stretching of NO_2 group [55], indicating surface covering. The presence of 0.23% \pm 0.02% in mass nitrogen was found by CHNS analysis. Since there isn't the possibility of doping, according to XRD analysis, we can suppose that the nitrogen is dispersed in the materials surface, which is in accordance to the FTIR analysis, where the band at 1,633 cm^{-1} was assigned to nitro groups. The occurrence of nitro groups in the materials surface is more pronounced in the samples submitted at 450°C. A higher annealing temperature (500°C) makes the intensity of this band in FTIR analysis lower, indicating the elimination of adsorbed NO_2 onto

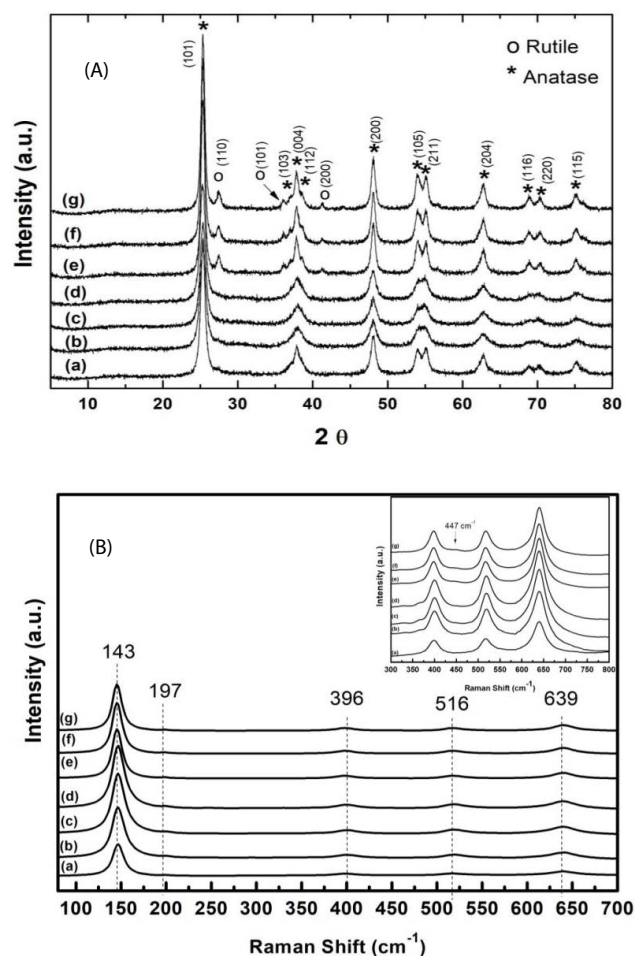


Fig. 1. (A) X-ray diffraction patterns and (B) Raman spectra between 70 and 700 cm^{-1} of TiO_2 and N- TiO_2 powders submitted to heat treatment: (a) TiO_2 , (b) 450TiN2, (c) 450TiN12, (d) 450TiN24, (e) 500TiN2, (f) 500TiN12, and (g) 500TiN24.

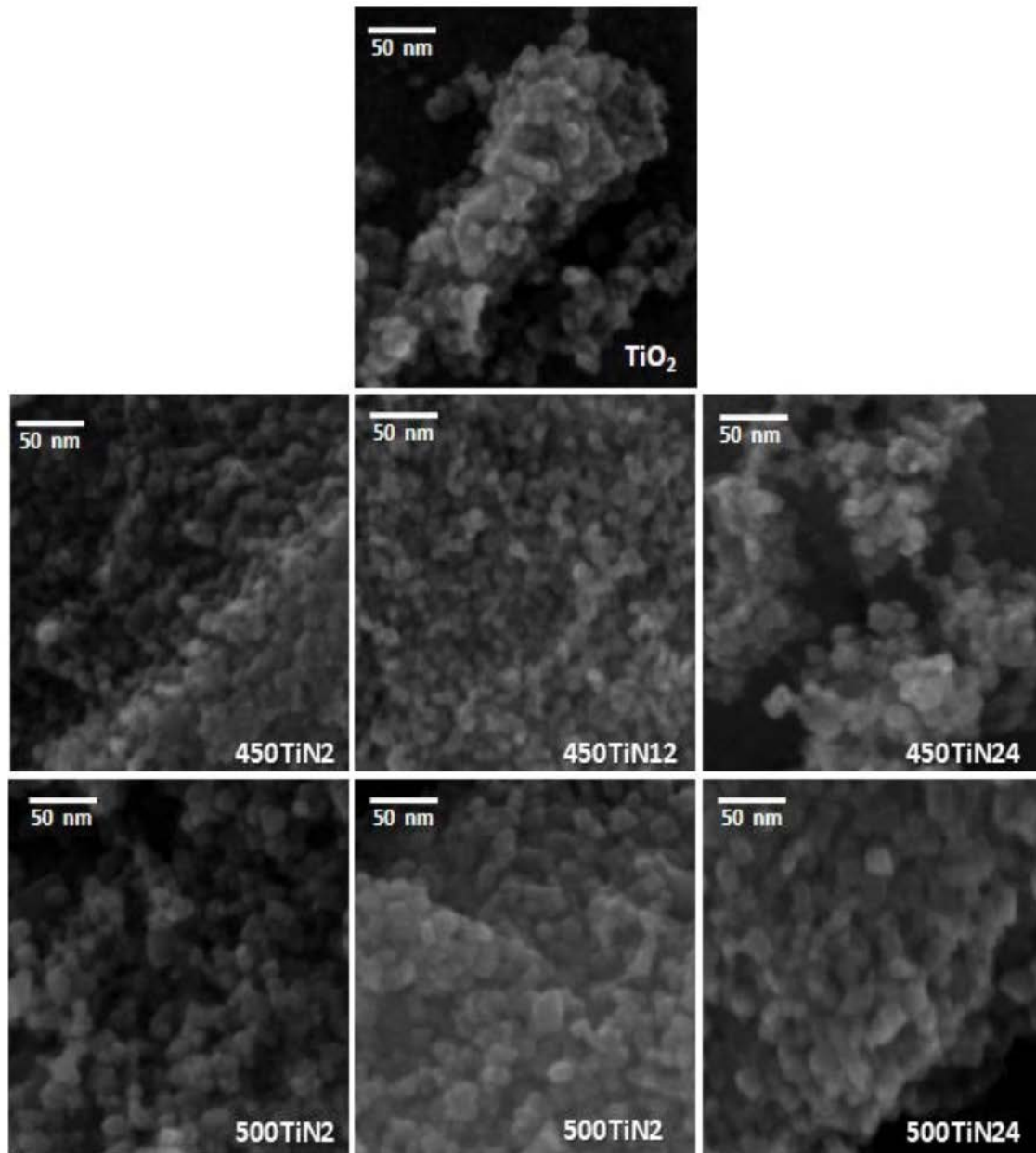


Fig. 2. FEG images of TiO_2 and N- TiO_2 nanoparticles obtained at different temperatures.

Table 1
Crystallite size and particles size of TiO_2 and N- TiO_2

Sample	Crystallite size (nm)	Particle size (nm)
TiO_2	13	15
450TiN2	8	10
450TiN12	8	10
450TiN24	8	20
500TiN2	12	15
500TiN12	13	20
500TiN24	13	25

materials surface. Correlating these results with particle size of TiO_2 and 450TiN12 sample, it is possible to conclude that these groups on the surface avoid the growth of particles, since it does not allow the contact between them.

Diffuse reflectance data (Fig. 3b) confirm that the material obtained was not doped with the nitrogenous, in the sense that no changes were found in the light absorption region (360 nm for all samples analyzed). The bandgap is approximately 2.91 ± 0.01 eV for all samples, showing no significant variation. Thus, it can be stated that the nitrogen quantified by CHNS is on the surface of the material, probably in the form of nitro groups, as suggested by the FTIR results.

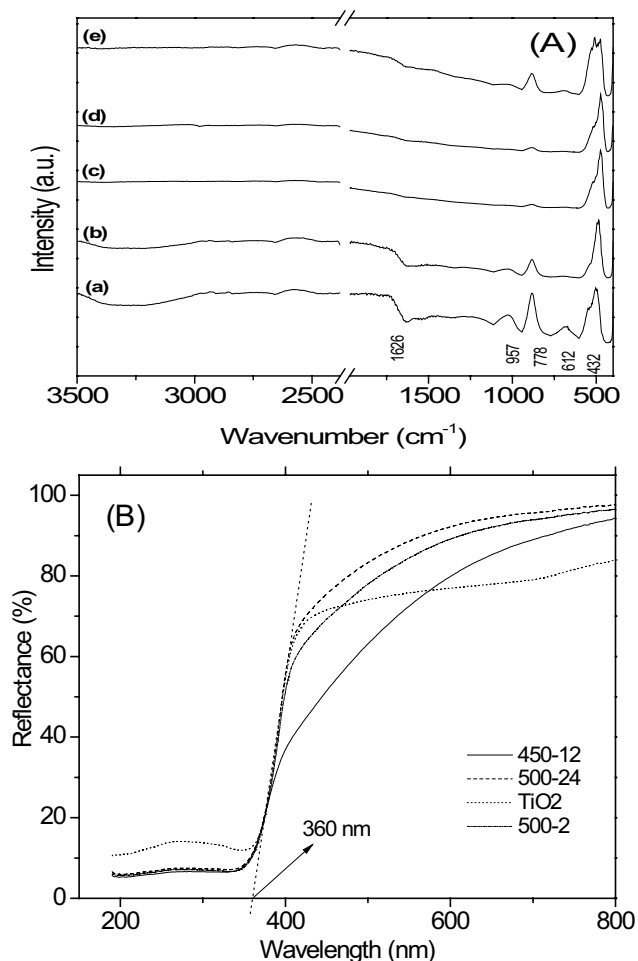


Fig. 3. (A) Infrared spectra of the samples: (a) 450TiN₂, (b) 450TiN₁₂, (c) 500TiN₂, (d) 500TiN₁₂, (e) 500TiN₂₄, and (B) diffuse reflectance.

3.2. Photocatalytic efficiency

Photocatalytic efficiency of the samples were tested against two different compounds, RhB dye and FLX, both under UV light. Fig. 4 shows the color removal in RhB solution with exposure time. It can be seen that all the samples were able to catalyze the process, since the decay in the concentration of RhB was faster compared to the blank.

TiO₂ surface modification yielded in more effective samples, since N-TiO₂ showed better performance than bare TiO₂. It is interesting, since it has been reported that adsorbed species on the semiconductor surface decrease their photocatalytic efficiency, mainly due to the occupancy of active sites that would act in photocatalysis. For example, Giraldo et al. [17] synthesized ZnO nanoparticles using zinc sulfate as metal source. The samples presented residual sulfate groups on their surface, which showed a deleterious effect in the photocatalytic efficiency by isolating the particle surfaces and hindering their photocatalytic activity in 17% compared with ZnO samples without these species adsorbed on the surface. Gonçalves et al. [56] studied TiO₂ nanoparticles obtained by chemical route and verified that

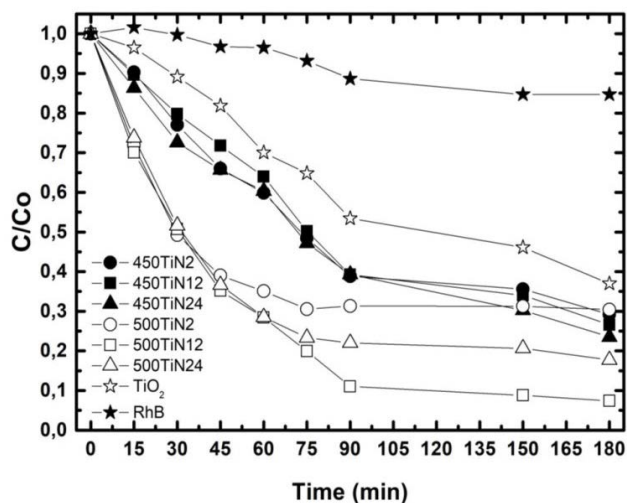


Fig. 4. Evolution of relative concentration of RhB as a function of irradiation time, under UV irradiation.

samples containing C–H species adsorbed on the semiconductor surface showed lower photoactivity. However, in this research, the photocatalytic activity of TiO₂ was significantly improved through surface modification with nitro groups.

In order to understand the improvement in photocatalytic activity of the samples presenting nitro groups on their surfaces, we performed zeta potential analysis. The improvement could be related to the fact that the nanoparticles covered with nitro groups presented more positive zeta potential than nanoparticles without nitro groups on the surface (+28 mV to TiO₂ and +34 mV to N-TiO₂). The more positive surface of modified TiO₂ can interact with the deprotonated carboxylic group from RhB. This interaction facility, improvement the photodegradation by dye sensitization or radical attack, which are the main mechanisms is RhB color removal [57]. In fact, literature reports that the degradation of RhB is more efficient in acid pH [58,59].

Besides, by comparing the samples photoactivity, it was observed that samples annealed at low temperatures are less effective than samples annealed at higher temperatures. An important point is the fact that samples annealed at higher temperatures presented a small amount of Rutile in the structure. It is reported in literature that a small amount of rutile phase in anatase nanocrystals presents a synergistic effect on the effectiveness of the materials, due to the heterojunction formation, which act maintaining the photogenerated charges physically separated, increasing their lifetimes and, consequently, the occurrence of redox reactions in the materials surface [60].

In order to study the applicability of the surface modified TiO₂ nanoparticles in different compounds, we used 450TiN₁₂ sample for FLX photodegradation. This sample was selected since it showed the best performance in RhB color removal under UV radiation. For comparison purposes, we also studied the performance of bare TiO₂ and the results are presented in Fig. 5a. It can be seen that the photocatalytic and photocatalytic processes using 450TiN₁₂ and TiO₂

samples under UV radiation presented the same efficiency. Therefore, we can conclude that the insertion of the photocatalysts in the system did not exert a positive influence on the degradation process of FLX in the conditions applied in this study. At this point, we highlight that the FLX molecule has a trifluoro group (with high negative charge density), as well as an amine group which, at values of $\text{pH} < 9$, are preferably in their protonated form [61,62]. These characteristics of the molecule influence its interaction with other materials/media, since the repulsion/attraction forces are dependent on the conditions of the reaction medium, as discussed in studies previous [61]. Thus, the indifference in the photodegradation efficiency of the FLX by means of the different nanomaterials can be associated with electrostatic repulsion between the molecule and nanoparticle.

In order to deep understand the process, we studied the FLX degradation mechanism by measuring the by-products formation during UV irradiation. Fig. 5b shows the formation of TFMP. Interestingly, when the surface modified nanoparticle was applied, the maximum amount of TFMP formed was lower ($1.4 \times 10^{-5} \text{ mol L}^{-1}$) when compared to the others systems, which the maximum amount of TFMP formed were 1.51×10^{-5} and $1.53 \times 10^{-5} \text{ mol L}^{-1}$ verified for the studies with TiO_2 and without nanomaterial, respectively.

It is also possible to verify that the dehalogenation process (Fig. 5c) is more efficient for the system without nanomaterial, where $1.56 \times 10^{-4} \text{ mol L}^{-1}$ of fluoride formation

is verified. The formation of 7.11×10^{-5} and $7.42 \times 10^{-5} \text{ mol L}^{-1}$ are observed in the photocatalytic studies using TiO_2 and 450TiN12, respectively, in the period of 120 min. Thus, the dehalogenation process is 52.4% smaller for photocatalytic processes when compared to the photolytic process.

According to data presented by Silva et al. [38] and Lam et al. [50], different mechanisms of degradation of FLX are presented, the by-products being halogenated, partially halogenated or totally dehalogenated. Since during the tests, TMPF, fluoride, and pH were monitored, it was possible to evaluate the stoichiometry of the process for photolytic and photocatalytic systems.

The TFMP byproduct is trihalogenated, and thus the formation of fluoride in the system can be the result of the degradation of this compound, which can occur through mono, di, or tri-dehalogenation. Considering the mechanism of mono-dehalogenated by-product formation, we have:



Applying 1:1 stoichiometry for the entire process, we have:

$$[\text{Fluoride}]_{\text{Formed}} = [\text{TFMP}]_{\text{degraded}} \quad (3)$$

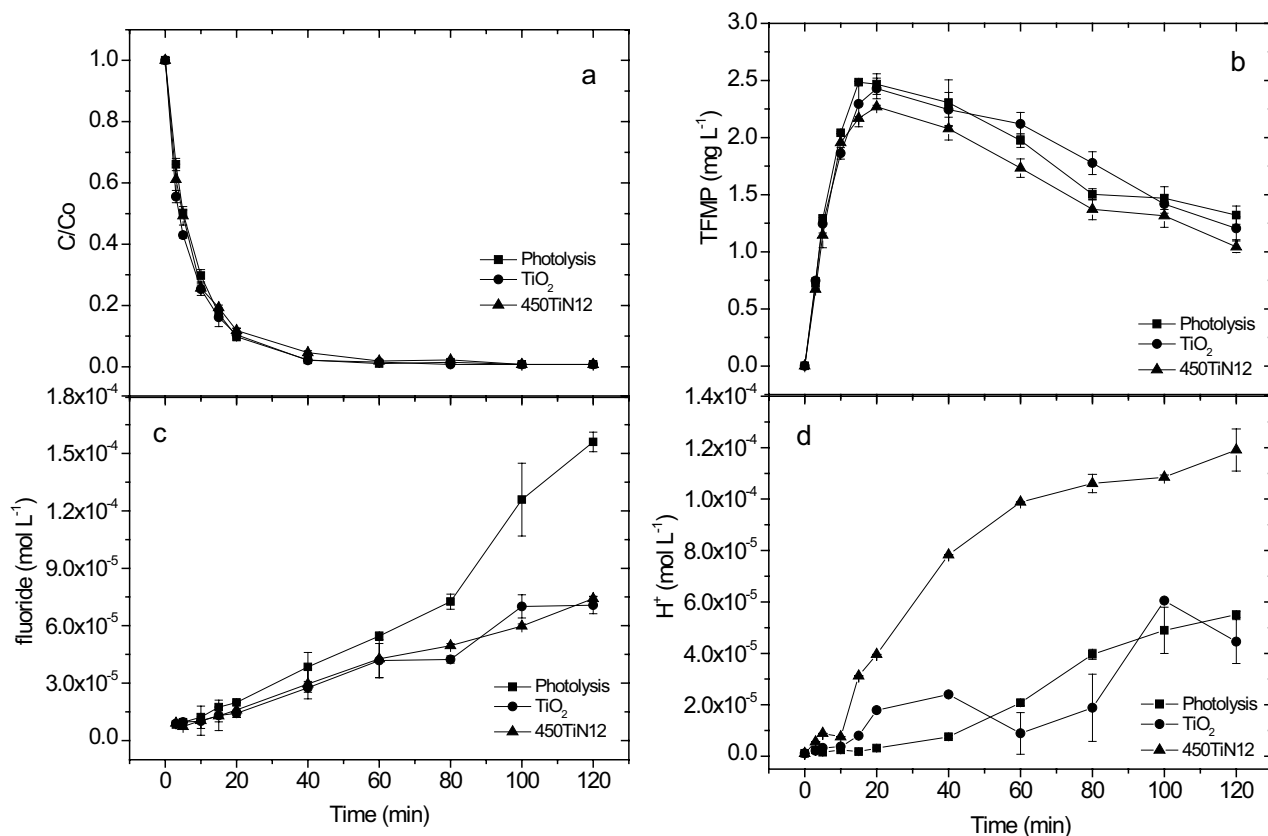


Fig. 5. Photolytic and photocatalytic degradation rate of FLX (a) and quantitative variation of formation of TFMP (b), fluoride (c) and H^+ ions (d).

and in this way

$$[\text{TFMP}]_{\text{Formed}} = [\text{TMFP}]_{\text{Present}}^* + [\text{Fluoride}]_{\text{Formed}} \quad (4)$$

*TFMP remaining in the system after irradiation.

Fig. 6a shows the stoichiometric relationship between the degraded FLX and the TFMP formed for the photolytic and photocatalytic processes, where an equivalence up to the time of 20 min is verified (Fig. 6b). After this period, the degradation of FLX is above 90%, and the degradation of TFMP formed is verified with greater evidence, that is, the 1:1 stoichiometric ratio is no longer applicable after 20 min.

It is important to note that the FLX degradation process needs to be evaluated in two steps. Through Fig. 5, we observed similar behaviors in terms of FLX degradation, formation of TFMP and fluoride up to the first 20 min (step 1) and different behaviors after 20 min (step 2). Thus, in terms of dehalogenation, we can say that this can occur for both FLX and TFMP (both are halogenated compounds), but it should be clear that up to 20 min, the conversion rates from FLX to TFMP are 93% (UV), 77% (TiO_2), and 79% (450TiN12), which leads us to conclude that exist the change in the mechanism through the insertion of semiconductors.

Figs. 5b and c show that the behavior of the TFMP and fluoride variation is not significantly influenced by the different processes (with the exception of dehalogenation in the photolytic process). Thus, it can be attributed that the greater dehalogenation in direct photolysis is related to the degradation mechanism of FLX that was not converted to TFMP (7% of FLX). According to Lam et al. [50], the FLX can undergo photonucleophilic substitution, where the $-\text{CF}_3$ group is substituted by the $-\text{COOH}$ group, allowing a greater release of fluorine in the system (the dehalogenation of FLX would follow a stoichiometry of 1:3).

In order to obtain a better understanding of these mechanisms, pH monitoring was performed (Fig. 5d), which showed a high influence of the nitro groups present on the TiO_2 surface. For photolytic and photocatalytic processes with TiO_2 , a similar behavior was observed in the deprotonation rate for the time interval up to 120 min. When the degradation processes without nanomaterial and with TiO_2 were compared with the nanomaterial containing the nitro group, a mean increase in deprotonation above 100% was observed. Thus, the first conclusion we have is that the UV process promotes dehalogenation, the 450TiN12 process promotes deprotonation, and the TiO_2 process exerts no comparative influences on the processes mentioned above.

The high deprotonation associated with the photocatalytic process using 450TiN12 can be attributed to the presence of the nitro group on the surface of the nanomaterial, as evidenced by the absorption range ($1,633 \text{ cm}^{-1}$) observed in Fig. 3. According to Rosseler et al. [63], the nitro group (NO_2) adsorbed on TiO_2 anatase is capable of abstracting the photogenerated electron from the semiconductor when irradiated in the UV region. As the 450TiN12 semiconductor presents the nitro group of surface, the electron abstraction can be attributed, however, this electron does not originate only from the possible electronic excitation of

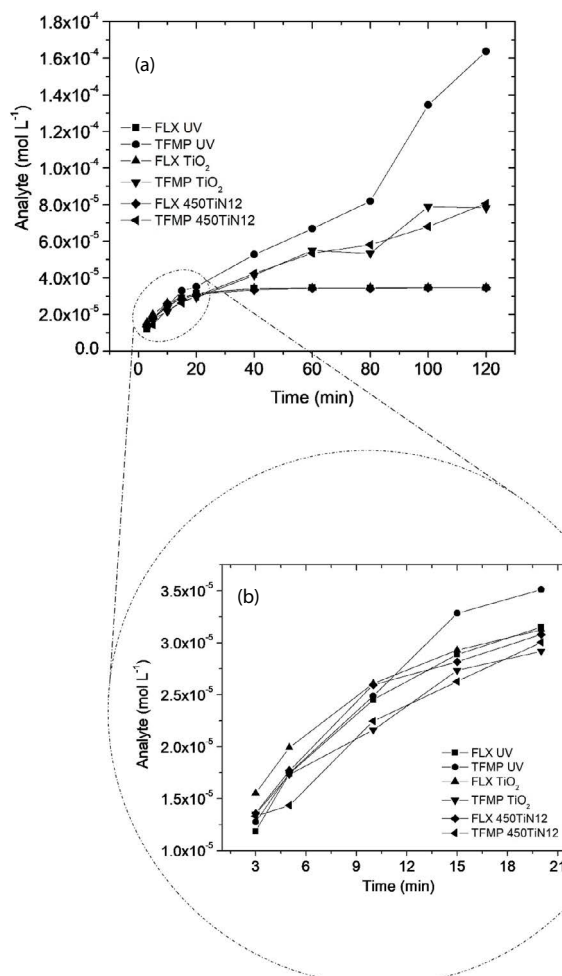


Fig. 6. Molar concentration data of FLX and TFMP when applied at stoichiometry from 1:1 to 120 min (a) and 20 min (b) of reaction. The curves that represent the FLX degradation are verified with increasing behavior, so, for the sake of clarity, these lines were obtained by: $[\text{FLX}]_{\text{degraded}} = [\text{FLX}]_0 - [\text{FLX}]_t$. This procedure was adopted so that the relation between the stoichiometric proportions between FLX and TFMP in the different systems was better correlated.

TiO_2 (anatase), since the FLX has a secondary amino group (nucleophile) [48,64].

The influence of pH was evaluated by Zhao et al. [48], during the FLX degradation process, it being verified that, because it has a $\text{p}K_a = 8.7\text{--}10.1$ [65,66], FLX can be present in its protonated form at $\text{pH} < 3$ and deprotonated to $\text{pH} > 11$, and the predominance of the protonated form at neutral pH was verified (neutral pH was applied in this study). Considering that the FLX samples are protonated, the loss of the hydronium occurs in the presence of a stronger electrophile, which was confirmed for the 450TiN12 semiconductor, where this electrophile is the nitro group of surface.

Thus, the interaction of the nucleophile (FLX amino group) with the electrophile (nitro group of the nanomaterial) promotes the deprotonation of the FLX, decreasing the pH in the system when the 450TiN12 process is applied.

Therefore, we can conclude that the ether bond divided the molecule (FLX) into two distinct reactive moieties in this study, where the halogenated portion reacted preferentially by direct photolysis, and the portion containing the amino group interacted preferentially through TiO_2 -N photocatalysis, promoting deprotonation.

The non-effectiveness of TiO_2 in the processes of dehalogenation and/or deprotonation is due to the fact that the nanomaterial does not promote the electron conduction of the valence band to the conduction band (internal recombination), nor does it present the superficial nitro groups, responsible for influencing the deprotonation of the amino group of FLX.

Considering a 1:1 stoichiometry, the rate of degradation of FLX and TFMP formation must follow the same kinetic order. The data in Table 2, showed the kinetic constant and their respective linear correlation coefficients. The kinetic data show that the rate of degradation of FLX and formation of TFMP do not present significant variations for the different processes.

Continuing the understanding of the degradation mechanism for the different processes, it was verified that the

formation of fluoride and H^+ ions also follows a kinetics of formation of pseudo-first-order. The data of formation, constant for Fluoride and H^+ ions (Table 2), show that the kinetic constants of fluoride formation were 89% and 23% higher for the UV process than the values for TiO_2 and 450TiN12, respectively, indicating that the insertion of nanomaterial, inhibits dehalogenation.

The data on the deprotonation process (H^+ ion formation) show that the kinetic constant for the N-450TiN12 process is 4% higher than that observed for the TiO_2 process, and comparing with the results presented in Fig. 5d, we can conclude that the presence of nitro group exerts greater influence on the deprotonation mechanism.

The discussion and interpretation of the data obtained in this work allows to suggest the mechanism of degradation of FLX, according to Fig. 7, where all the suggested compounds are reported in the literature by Silva et al. [38] and Lam et al. [50]. This study reports qualitative and quantitative data that suggest a direct photolytic mechanism and a photocatalytic mechanism (Fig. 7).

Finally, it is important to note that the performance of nanomaterials in chemical processes must be observed

Table 2

Kinetic data of pseudo-first-order degradation of FLX and formation of TFMP, fluoride, and H^+ ions for the first 20 min of reaction applied to stoichiometry of 1: 1

Catalyst	FLX degradation k (min^{-1})/ R^2	TFMP formation k (min^{-1})/ R^2	H^+ ion k (min^{-1})/ R^2	Fluoride k (min^{-1})/ R^2
–	0.110/0.999	0.054/0.886	–	0.053/0.975
TiO_2	0.097/0.996	0.044/0.905	0.118/0.943	0.028/0.933
450TiN12	0.090/0.977	0.050/0.922	0.123/0.966	0.043/0.963

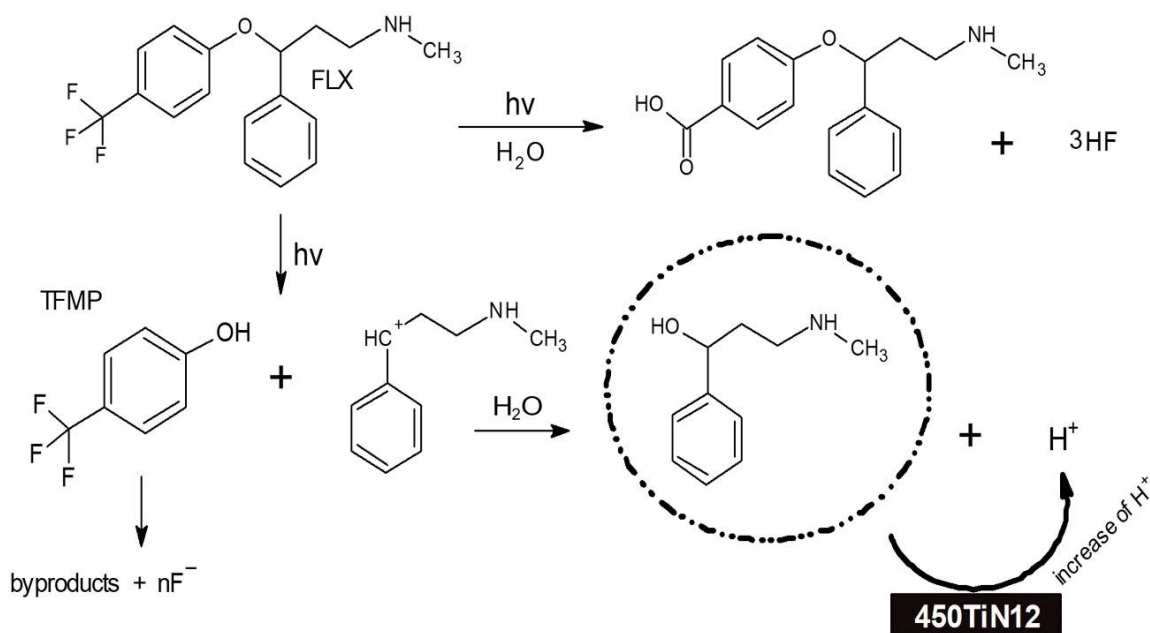


Fig. 7. Mechanism of degradation of FLX and formation of TFMP, fluoride, and H^+ ions applying the stoichiometry of 1:1:1:1 (FLX:TFMP:Fluoride: H^+) up to 20 min of reaction. Adapted from Lam et al. [50].

beyond the degradation of the original compound, since the selectivity and influence on the degradation mechanisms of the by-products can contribute to the obtaining of more accessible routes to the human needs, environmental, pharmaceutical, medical, or general chemistry.

4. Conclusion

In this research, we showed the synthesis and photocatalytic properties of surface modified TiO₂ nanoparticles. The insertion of nitro groups on the materials surface was confirmed by different techniques, showing that the synthesis method applied in this work was able to promote modifications on the materials surface that improves their photocatalytic properties against RhB dye under UV light. Two effects were listed as important to tailor the photocatalytic efficiency of the materials, the nitro groups on the materials surface and the occurrence of second phase in anatase structure, which can act as repository of photogenerated charges, increasing their lifetimes and the rate of redox reactions over materials surface. To further investigate the as synthesized samples in different systems, FLX photodegradation was studied. The monitoring of degradation by-products (TFMP and fluoride) allowed to define the stoichiometry of the reaction. The influence of the catalysts on the drug degradation mechanism is significant for the deprotonation process, indicating that the nitro groups (electrophiles), interact with the amino group (nucleophilic) of the FLX/by-products, causing their deprotonation and decreasing the pH of the medium. Despite the fact the FLX degradation rate wasn't improved, the results presented here regarding the mechanism of degradation in presence of nanoparticles can be used in the design of alternative materials to be applied in several systems.

Acknowledgments

The financial backing of the Brazilian agency CAPES, FAPEMIG (process number: APQ-02823-14), and CNPq (proc. 444117/2014-8 and proc. 409904/2019-3) is gratefully acknowledged.

References

- [1] S.W. Kim, M. Kim, W.Y. Lee, T. Hyeon, Fabrication of hollow palladium spheres and their successful application to the recyclable heterogeneous catalyst for suzuki coupling reactions, *J. Am. Chem. Soc.*, 124 (2002) 7642–7643.
- [2] F. Caruso, Hollow capsule processing through colloidal templating and self-assembly, *Chem. Eur. J.*, 6 (2000) 413–419.
- [3] M. Zhang, G. Gao, D.C. Zhao, Y.Z. Li, F.Q. Liu, Crystallization and photovoltaic properties of titania-coated polystyrene hybrid microspheres and their photocatalytic activity, *J. Phys. Chem. B*, 109 (2005) 9411–9415.
- [4] H. Nakamura, M. Ishii, A. Tsukigase, M. Harada, H. Nakano, Close-packed colloidal crystalline arrays composed of polystyrene latex coated with titania nanosheets, *Langmuir*, 21 (2005) 8918–8922.
- [5] J. Li, H.C. Zeng, Size tuning, functionalization, and reactivation of Au in TiO₂ nanoreactors, *Angew. Chem. Int. Ed.*, 44 (2005) 4342–4345.
- [6] Y.Z. Li, H. Zhang, X.L. Hu, X.J. Zhao, M. Han, Efficient visible-light-induced photocatalytic activity of a 3D-ordered titania hybrid photocatalyst with a core/shell structure of dye containing polymer/titania, *J. Phys. Chem. C*, 112 (2008) 14973–14979.
- [7] K. Kondo, H. Yoshikawa, K. Awaga, M. Murayama, T. Mori, K. Sunada, S. Bandow, S. Iijima, Preparation, photocatalytic activities, and dye-sensitized solar-cell performance of submicron scale TiO₂ hollow spheres, *Langmuir*, 24 (2008) 547–550.
- [8] G.S. Nascimento, G.P. Mambrini, E.C. Paris, J.A. Peres, L.A. Colnago, C. Ribeiro, Evaluation of the catalytic activity of oxide nanoparticles synthesized by the polymeric precursor method on biodiesel production, *J. Mater. Res.*, 27 (2012) 3020–3026.
- [9] M.A. Fox, M.T. Dulay, Heterogeneous photocatalysis, *Chem Rev.*, 93 (1993) 341–357.
- [10] A.J. Moreira, A.C. Borges, L.F.C. Gouvea, T.C.O. MacLeod, G.P.G. Freschi, The process of atrazine degradation, its mechanism, and the formation of metabolites using UV and UV/MW photolysis, *J. Photochem. Photobiol., A*, 347 (2017) 160–167.
- [11] W.K. Wang, J.J. Chen, M. Gao, Y.X. Huang, X. Zhang, H.Q. Yu, Photocatalytic degradation of atrazine by boron-doped TiO₂ with a tunable rutile/anatase ratio, *Appl. Catal., B*, 195 (2016) 69–76.
- [12] Y. Zhang, J. Li, L. Zhou, G. Wang, Y. Feng, Z. Wang, X. Yang, Aqueous photodegradation of antibiotic florfenicol: kinetics and degradation pathway studies. *Environ. Sci. Pollut. Res.*, 23 (2016) 6982–6989.
- [13] H.W. Yu, T. Anumol, M. Park, I. Pepper, J. Scheideler, S.A. Snyder, On-line sensor monitoring for chemical contaminant attenuation during UV/H₂O₂ advanced oxidation process, *Water Res.*, 81 (2015) 250–260.
- [14] C. Amorim, M.A. Keane, Effect of surface acid groups associated with amorphous and structured carbon on the catalytic hydrodechlorination of chlorobenzenes, *Chem. Technol. Biotechnol.*, 83 (2008) 662–672.
- [15] G. Xiong, X. Wang, L.D. Lu, X.J. Yang, Y.F. Xu, Preparation and characterization of Al₂O₃-TiO₂ composite oxide nanocrystals, *J. Solid State Chem.*, 141 (1998) 70–77.
- [16] V.R. Mendonça, C. Ribeiro, Influence of TiO₂ morphological parameters in dye photodegradation: a comparative study in peroxo-based synthesis, *Appl. Catal., B*, 105 (2011) 298–305.
- [17] T.R. Giraldi, G.V.F. Santos, V.R. Mendonça, C. Ribeiro, I.T. Weber, Effect of synthesis parameters on the structural characteristics and photocatalytic activity of ZnO, *Mater. Chem. Phys.*, 136 (2012) 505–511.
- [18] M. Anpo, Use of visible light. Second-generation titanium oxide photocatalysts prepared by the application of an advanced metal ion-implantation method, *Pure Appl. Chem.*, 72 (2000) 1787–1792.
- [19] A. Di Paola, G. Marci, L. Palmisano, M. Schiavello, K. Uosaki, S. Ikeda, B. Ohtani, Preparation of polycrystalline TiO₂ photocatalysts impregnated with various transition metal ions: characterization and photocatalytic activity for the degradation of 4-nitrophenol, *J. Phys. Chem. B*, 106 (2002) 637–645.
- [20] C.S. Enache, J. Schoonman, R.V. Krol, Addition of carbon to anatase TiO₂ by *n*-hexane treatment—surface or bulk doping? *Appl. Surf. Sci.*, 252 (2006) 6342–6349.
- [21] M. Janus, B. Tryba, M. Inagaki, A.W. Morawski, New preparation of a carbon-TiO₂ photocatalyst by carbonization of *n*-hexane deposited on TiO₂, *Appl. Catal., B*, 52 (2004) 61–67.
- [22] A. Abdelhaleem, W. Chu, Photodegradation of 4-chlorophenoxyacetic acid under visible LED activated N-doped TiO₂ and the mechanism of stepwise rate increment of the reused catalyst, *J. Hazard. Mater.*, 338 (2017) 491–501.
- [23] I. Jang, H.J. Leong, H. Noh, T. Rang, S. Kong, S.G. Oh, Preparation of N-functionalized TiO₂ particles using one-step sol-gel method and their photocatalytic activity, *J. Ind. Eng. Chem.*, 37 (2016) 380–389.
- [24] T. Umebayashi, T. Yamaki, H. Itoh, K. Assai, Band gap narrowing of titanium dioxide by sulfur doping, *Appl. Phys. Lett.*, 81 (2002) 454–456.

- [25] T. Ohno, Preparation of visible light active S-doped TiO₂ photocatalysts and their photocatalytic activities, *Water Sci. Technol.*, 49 (2004) 159–163.
- [26] I.T. Weber, A. Valentini, L.F.D. Probst, E. Longo, E.R. Leite, Influence of noble metals on the structural and catalytic properties of Ce-doped SnO₂ systems, *Sens. Actuators, B*, 97 (2004) 31–38.
- [27] D.A. Duarte, M. Massi, A.S.S. Sobrinho, Development of dye-sensitized solar cells with sputtered N-doped thin films: from modeling the growth mechanism of the films to fabrication of the solar cells, *Int. J. Photoenergy*, 2014 (2014) 13 p, doi: 10.1155/2014/839757.
- [28] D.W. Chen, A.K. Ray, Photocatalytic kinetics of phenol and its derivatives over UV irradiated TiO₂, *Appl. Catal., B*, 23 (1999) 143–157.
- [29] A. Fujishima, N. Rao, D.A. Tryk, Titanium dioxide photocatalysis, *J. Photochem. Photobiol., C*, 1 (2000) 1–21.
- [30] S.H. Bossmann, S. Göb, T. Siegenthaler, A.M. Braun, K.T. Ranjit, I. Willner, An N,N'-dialkyl-4,4'-bipyridinium-modified titanium-dioxide photocatalyst for water remediation – observation and application of supramolecular effects in photocatalytic degradation of π -donor organic compounds, *Fresenius J. Anal. Chem.*, 371 (2001) 621–628.
- [31] I.G. Juan, L. Macé, S. Tengeler, A. Mosallem, N. Nicoloso, R. Riedel, Photoluminescence of urea- and urea/rhodamine B-capped TiO₂ nanoparticles, *Mater. Chem. Phys.*, 177 (2016) 472–478.
- [32] B. Yao, C. Peng, P. Lu, Y. He, W. Zhang, Q. Zhang, Fabrication of Tiron-TiO₂ charge-transfer complex with excellent visible-light photocatalytic performance, *Mater. Chem. Phys.*, 184 (2016) 298–305.
- [33] B. Tryba, A.W. Morawski, M. Inagaki, Application of TiO₂-mounted activated carbon to the removal of phenol from water, *Appl. Catal., B*, 41 (2003) 427–433.
- [34] L.S. Xing, Z.F. Ying, C.W. Lian, H.A. Qin, X.Y. Kun, Surface modification of nanometer size TiO₂ with salicylic acid for photocatalytic degradation of 4-nitrophenol, *J. Hazard. Mater.*, 135 (2006) 431–436.
- [35] K. Hadjiivanov, V. Bushev, M. Kantcheva, D. Klissurski, Infrared spectroscopy study of the species arising during NO₂ adsorption on TiO₂ (Anatase), *Langmuir*, 10 (1994) 464–471.
- [36] L. Zhang, J.M. Cole, Can nitro groups really anchor onto TiO₂? Case study of dye-to-TiO₂ adsorption using azo dyes with NO₂ substituents, *Phys. Chem. Chem. Phys.*, 18 (2016) 19062–9069.
- [37] Z. Pap, L. Baia, K. Mogyorósi, A. Dombi, A. Oszkó, V. Danciu, Correlating the visible light photoactivity of N-doped TiO₂ with brookite particle size and bridged-nitro surface species, *Catal. Commun.*, 17 (2012) 1–7.
- [38] V.H.O. Silva, A.P.S. Batista, A.C.S. Teixeira, S.I. Borrelly, Degradation and acute toxicity removal of the antidepressant Fluoxetine (Prozac®) in aqueous systems by electron beam irradiation, *Environ. Sci. Pollut. Res.*, 23 (2016) 11927–11936.
- [39] D.C. Thompson, K. Perera, R. London, Spontaneous hydrolysis of 4-trifluoromethylphenol to a quinone methide and subsequent protein alkylation, *Chem. Biol. Interact.*, 126 (2000) 1–14.
- [40] H. Hidaka, T. Tsukamoto, T. Oyama, Y. Mitsutsuka, T. Takamura, N. Serpone, Photoassisted defluorination of fluorinated substrates and pharmaceuticals by a wide bandgap metal oxide in aqueous media, *Photochem. Photobiol. Sci.*, 12 (2013) 751–759.
- [41] B.V. Pinto, A.P.G. Ferreira, E.T.G. Cavalheiro, A mechanism proposal for fluoxetine thermal decomposition, *J. Therm. Anal. Calorim.*, 130 (2017) 1553–1559.
- [42] L. Yin, R. Ma, B. Wang, H. Yuan, G. Yu, The degradation and persistence of five pharmaceuticals in an artificial climate incubator during a one year period, *RSC Adv.*, 7 (2017) 8280–8287.
- [43] W.L. Silva, M.A. Lansarin, P.R. Livotto, J.H.Z. Santos, Photocatalytic degradation of drugs by supported titania-based catalysts produced from petrochemical plant residue, *Powder Technol.*, 279 (2015) 166–172.
- [44] M.A. Sousa, C. Gonçalves, V.J.P. Vilar, R.A.R. Boaventura, M.F. Alpendurada, Suspended TiO₂-assisted photocatalytic degradation of emerging contaminants in a municipal WWTP effluent using a solar pilot plant with CPCs, *Chem. Eng. J.*, 198–199 (2012) 301–309.
- [45] N.F.F. Moreira, J.M. Sousa, G. Macedo, A.R. Ribeiro, L. Barreiros, M. Pedrosa, J.L. Faria, M.F.R. Pereira, S.C. Silva, M.A. Segundo, C.M. Manaia, O.C. Nunes, A.M.T. Silva, Photocatalytic ozonation of urban wastewater and surface water using immobilized TiO₂ with LEDs: micropollutants, antibiotic resistance genes and estrogenic activity, *Water Res.*, 94 (2016) 10–22.
- [46] A. Hu, X. Zhang, D. Luong, K.D. Oakes, M.R. Servos, R. Liang, R. Kurdi, P. Peng, Y. Zhou, Adsorption and photocatalytic degradation kinetics of pharmaceuticals by TiO₂ nanowires during water treatment, *Waste Biomass Valorization*, 3 (2012) 443–449.
- [47] M.F. Arriaga, T. Otsu, T. Oyama, J. Gimenes, S. Esplugas, H. Hidaka, N. Serpone, Photooxidation of the antidepressant drug Fluoxetine (Prozac) in aqueous media by hybrid catalytic/ozonation processes, *Water Res.*, 45 (2011) 2782–2794.
- [48] Y. Zhao, G. Yu, S. Chen, S. Zhang, B. Wang, J. Huang, S. Deng, Y. Wang, Ozonation of antidepressant fluoxetine and its metabolite product norfluoxetine: kinetics, intermediates and toxicity, *Chem. Eng. J.*, 316 (2017) 951–963.
- [49] C. Salazar, C. Ridruejo, E. Brillas, J. Yáñez, H.D. Mansilla, I. Sirés, Abatement of the fluorinated antidepressant fluoxetine (Prozac) and its reaction by-products by electrochemical advanced methods, *Appl. Catal., B*, 203 (2017) 189–198.
- [50] M. Lam, C. Young, S. Mabury, Aqueous photochemical reaction kinetics and transformations of fluoxetine, *Environ. Sci. Technol.*, 39 (2005) 513–522.
- [51] J.N. Sahu, A.V. Patwardhan, B.C. Meikap, *In-situ* catalytic synthesis of ammonia from urea in a semi-batch reactor for safe utilization in thermal power plant, *Asia-Pac. J. Chem. Eng.*, 5 (2010) 533–543.
- [52] M.A. Kebede, M.E. Varner, N.K. Scharko, N.B. Gerber, J.D. Raff, Photooxidation of ammonia on TiO₂ as a source of NO and NO₂ under atmospheric conditions, *J. Am. Chem. Soc.*, 135 (2013) 8606–8615.
- [53] M. Kakihana, Invited review “sol-gel” preparation of high temperature superconducting oxides, *J. Sol-Gel Sci. Technol.*, 6 (1996) 7–55.
- [54] G.B. Soares, B. Bravin, C.M.P. Vaza, C. Ribeiro, Facile synthesis of N-doped TiO₂ nanoparticles by a modified polymeric precursor method and its photocatalytic properties, *Appl. Catal., B*, 106 (2011) 287–294.
- [55] R.M. Silverstein, F.X. Webster, D.J. Kiemle, *Spectrometric Identification of Organic Compounds*, 7th ed., State University of New York, New York, NY, 2005.
- [56] P. Gonçalves, R. Bertholdo, J.A. Dias, S.C. Maestrelli, T.R. Giraldo, Evaluation of the photocatalytic potential of TiO₂ and ZnO obtained by different wet chemical methods, *Mater. Res.*, 20 (2017) 181–189.
- [57] V.R. Mendonça, H.A.J.L. Mourão, A.R. Malagutti, C. Ribeiro, The role of the relative dye/photocatalyst concentration in TiO₂ assisted photodegradation process, *Photochem. Photobiol.*, 90 (2014) 66–72.
- [58] C. Wang, Y. Zhang, L. Yu, Z. Zhang, H. Sun, Oxidative degradation of azo dyes using tourmaline, *J. Hazard. Mater.*, 260 (2013) 851–859.
- [59] Y. Zhou, X.J. Zhang, Z. Zhao, Q. Zhang, F. Wang, Y. Lin, Effects of pH on the visible-light induced photocatalytic and photoelectrochemical performances of hierarchical Bi₂WO₆ microspheres, *Superlattices Microstruct.*, 72 (2014) 238–244.
- [60] R. Qian, H. Zong, J. Schneider, G. Zhou, T. Zhao, Y. Li, J. Yang, D.W. Bahnemann, J.H. Pan, Charge carrier trapping, recombination and transfer during TiO₂ photocatalysis: an overview, *Catal. Today*, 30 (2019) 78–90.
- [61] T.T.T. Do, U.P.N. Daa, H.T. Buib, T.T. Nguyen, Effect of electrostatic interaction between fluoxetine and lipid membranes on the partitioning of fluoxetine investigated using

- second derivative spectrophotometry and FTIR, *Chem. Phys. Lipids*, 207 (2017) 10–23.
- [62] E.S. Papas, C.N. Chaldezios, J.A. Politou, M.A. Koupparis, Construction of a fluoxetine ion chemical sensor and its application for the determination of pka value of fluoxetine conjugated acid, complexation study with b-cyclodextrin and formulations assay, *Anal. Lett.*, 43 (2010) 2171–2183.
- [63] O. Rosseler, M. Sleiman, V.N. Montesinos, A. Shavorskiy, V. Keller, N. Keller, M.I. Litter, H. Bluhm, M. Salmeron, H. Destailats, Chemistry of NO_x on TiO₂ surfaces studied by ambient pressure XPS: products, effect of UV irradiation, water, and coadsorbed K⁺, *J. Phys. Chem. Lett.*, 4 (2013) 536–541.
- [64] A.V. Tyntsunik, S.O. Kokhan, Y.M. Ivon, I.V. Komarov, O.O. Grygorenko, Intramolecular functional group differentiation as a strategy for the synthesis of bridged bicyclic β-amino acids, *RSC Adv.*, 6 (2016) 22737–22748.
- [65] S.A. Snyder, S. Adham, A.M. Redding, F.S. Cannon, J. De Carolis, J. Oppenheimer, E.C. Wert, Y. Yoon, Role of membranes and activated carbon in the removal of endocrine disruptors and pharmaceuticals, *Desalination*, 202 (2007) 156–181.
- [66] M. Bedner, W.A. MacCrehan, Reactions of the amine-containing drugs fluoxetine and metoprolol during chlorination and dechlorination processes used in wastewater treatment, *Chemosphere*, 65 (2006) 2130–2137.